Complete solution of the XXZ-model on finite rings; dynamical structure factors at zero temperature

1995 J. Phys.: Condens. Matter 7 5629

(http://iopscience.iop.org/0953-8984/7/28/017)

J. Phys.: Condens. Matter 7 (1995) 5629–5641. Printed in the UK

Complete solution of the *XXZ*-model on finite rings; dynamical structure factors at zero temperature

K Fabricius†§, K-H Mütter†‖ and U Löw§¶

† Physics Department, University of Wuppertal, 42097 Wuppertal, Germany
‡ Institut für Physik, Universität Dortmund 44221 Dortmund, Germany

Received 21 February 1995

Abstract. The finite-size effects of the dynamical structure factors in the *XXZ*-model are studied in the euclidean time (τ-) representation. Away from the critical momentum $p = \pi$ finite-size effects turn out to be small except for in large-τ limit. The large finite-size effects at the critical momentum $p = \pi$ signal the emergence of infrared singularities in the spectral (ω-) representation of the dynamical structure factors.

1. Introduction

Based on a complete diagonalization of the *XXZ*-Hamiltonian:

$$H = 2\sum_{x=1}^{N}[s_1(x)s_1(x+1) + s_2(x)s_2(x+1) + \cos\gamma s_3(x)s_3(x+1)] \qquad (1.1)$$

on finite rings with $N = 4, 6, \ldots, 16$ sites and anisotropy parameter $\gamma/\pi = 0.0, 0.1, 0.3, 0.4, 0.5$ we reported in [1] and [2] on the thermodynamics and the static structure factors at finite temperature. In this paper we continue our numerical investigation of the *XXZ*-model with an analysis of the dynamical structure factors:

$$\begin{aligned} S_j(\omega, p, T, \gamma, N) &= Z^{-1}\sum_n \delta(\omega - (E_n - E_m))\,\delta(p - p_n + p_m) \\ &\quad \times \exp\left(-\frac{E_m}{T}\right)|\langle n|s_j(0)|m\rangle|^2 \qquad j = 1, 3. \end{aligned} \qquad (1.2)$$

Z is the partition function and $|n\rangle$ denotes an eigenstate of the Hamilton operator and of the momentum operator with eigenvalues E_n and p_n, respectively. The dynamical structure factors contain the information on the transition probabilities $|\langle n|s_j(0)|m\rangle|^2$ between the eigenstates n and m with an excitation energy $\omega = E_n - E_m$ and a momentum transfer $p = p_n - p_m$. At $T = 0$ and $p = \pi$ the *XXZ*-model is known to be critical and here one expects that quantum effects become most important. Therefore, most of the previous studies were concentrated on the ground-state behaviour. There exist analytical results on the dynamical correlation functions for the special case $\gamma = \pi/2$, i.e for the *XX*-model

§ Klaus.Fabricius@wptu13.physik.uni-wuppertal.de.
‖ muetter@wpts0.physik.uni-wuppertal.de.
¶ loew@wptu14.physik.uni-wuppertal.de.

0953-8984/95/285629+13$19.50

[3–6]. This model can be mapped on a free fermion system [7] by means of a Jordan Wigner transformation. For the general case $0 \leqslant \gamma < \pi/2$, the spectrum of the low-lying excitation energies has been exploited by des Cloiseaux and Pearson [8]. In particular it was found from the Bethe *ansatz* solution that there is a lower bound

$$E_n - E_m \geqslant E_1(p_1, \gamma) - E_0(p_0, \gamma) = \omega_1(p, \gamma) = \frac{\pi}{\gamma} \sin\gamma \sin p \tag{1.3}$$

for the excitation energies depending on the momentum transfer $p = p_1 - p_0$. Approaching the boundary (1.3) the structure factors diverge [9]:

$$S_j(\omega, p, T = 0, \gamma, N = \infty) = A \frac{\Theta(\omega - \omega_1)}{(\omega^2 - \omega_1^2)^{\alpha_j(\gamma)}} \tag{1.4}$$

where

$$\alpha_1(\gamma) = \frac{1}{2}\left(1 + \frac{\gamma}{\pi}\right) \qquad \alpha_3(\gamma) = \frac{\pi/2 - \gamma}{\pi - \gamma}. \tag{1.5}$$

Starting from these rigorous results G Müller and collaborators [10] made an *ansatz* for the dynamical structure factors which has been applied successfully on the description of neutron scattering data [11].

The outline of the paper is as follows. In section 2 we present our results on the dynamical structure factors at $p = \pi$ and $N = 4, 6, \ldots, 16$. We make use of the euclidean time representation, which is particularly suited to analysing finite-size effects. In section 3 we demonstrate how infrared singularities emerge on finite systems. In section 4 we report on our results for noncritical momenta $p < \pi$.

2. Finite-size behaviour of the dynamical structure factors at $p = \pi$ and $T = 0$

In the critical regime:

$$p \to \pi \qquad T \to 0 \qquad N \to \infty \tag{2.1}$$

the dynamical structure factors (1.4) develop infrared singularities. We want to investigate how these singularities show up on finite systems, where the structure factors are sums of δ-function contributions. Finite-size effects are not so easy to analyse and we therefore look for a smoothening procedure which allows us to extract the thermodynamical limit from finite systems. For this purpose let us consider the Laplace transforms of the structure factors. At $T = 0$, $p = \pi$ they acquire the following form:

$$S_j(\tau, p = \pi, T = 0, \gamma, N) = \sum_{n>0} \delta(p_n - p_0 - \pi)\, \mathrm{e}^{-\tau(E_n - E_0)} |\langle n|s_j(0)|0\rangle|^2. \tag{2.2}$$

The variable τ can be interpreted as a euclidean time. At $\tau = 0$ we recover the static structure factors which behave for $N \to \infty$ as [12]:

$$S_j(\tau = 0, p = \pi, T = 0, \gamma, N \to \infty) = r_j(\gamma) \frac{\eta_j(\gamma)}{\eta_j(\gamma) - 1} \left[1 - \left(\frac{N}{N_j(\gamma)}\right)^{1-\eta_j(\gamma)}\right] \tag{2.3}$$

with critical exponents [9]:

$$\eta_1(\gamma) = \eta_3(\gamma)^{-1} = 1 - \frac{\gamma}{\pi}. \tag{2.4}$$

According to (2.3) and (2.4) the longitudinal structure factor stays finite whereas the transverse one diverges. This divergence originates from the infrared singularity (1.4) which is integrable for the longitudinal case ($2\alpha_3(\gamma) < 1$) but nonintegrable in the transverse case

($2\alpha_1(\gamma) > 1$). On finite systems the infrared singularities are not visible directly due to the gap:

$$\omega_1(p = \pi, \gamma, N) = E_1 - E_0 = O(N^{-1}) \tag{2.5}$$

between the ground-state energy E_0 and the energy E_1 of the first excited state. In the following we consider the Laplace transform (2.2) normalized to the corresponding static structure factor:

$$R_j(\tau, \gamma, N) = \frac{S_j(\tau, p = \pi, T = 0, \gamma, N)}{S_j(\tau = 0, p = \pi, T = 0, \gamma, N)} \qquad j = 1, 3. \tag{2.6}$$

By construction these ratios are monotonically decreasing with τ and varying between 1 and 0 for $\tau > 0$. Figures 1(a), (b), 2, 3(a), (b) present the ratio (2.6) for the longitudinal case at $\gamma/\pi = 0.5, 0.3$, the isotropic case $\gamma = 0$, and the transverse case at $\gamma/\pi = 0.3, 0.5$, respectively. Going from figure 1(a) to figure 3(b) we observe the following characteristic features:

(i) Finite-size effects are small in the longitudinal case at $\gamma/\pi = 0.5$ and increase with decreasing values of γ.

(ii) Finite-size effects are large in the transverse case and increase with increasing values of γ.

(iii) The 'half width' $\tau(R_j = 0.5, \gamma)$—defined as the value of τ, where the ratio (2.6) has dropped to $R_j = 0.5$—moves systematically:

$$\begin{aligned}\tau(R_3 = 0.5, \gamma = 0.5\pi) < \tau(R_3 = 0.5, \gamma = 0.3\pi) < \tau(R = 0.5, \gamma = 0) \\ < \tau(R_1 = 0.5, \gamma = 0.3\pi) < \tau(R_1 = 0.5, \gamma = 0.5\pi).\end{aligned} \tag{2.7}$$

As will be shown below, this property is related to the strengthening of the infrared singularity (1.4) according to (1.5):

$$\alpha_3(0.5\pi) < \alpha_3(0.3\pi) < \alpha(0) < \alpha_1(0.3\pi) < \alpha_1(0.5\pi).$$

The integrability of the infrared singularity in the Laplace transform (2.2) for the longitudinal case means that the ratio (2.6):

$$R_3(\tau, \gamma, N \to \infty) = R_3(\tau, \gamma) \tag{2.8}$$

converges to a scaling curve $R_3(\tau, \gamma)$. The large-τ behaviour of the scaling curve is given by the infrared singularity (1.4):

$$R_3(\tau, \gamma) \overset{\tau \to \infty}{\longrightarrow} \tau^{2\alpha_3 - 1}. \tag{2.9}$$

We have tried to determine the inverse $\tau = \tau(R_3, \gamma)$ of the scaling curve from a finite-size analysis of our results for $N = 4, 6, \ldots, 16$ with a parametrization:

$$\ln \tau(R_3, \gamma, N) = \ln \tau(R_3, \gamma) + \frac{B_3(R_3, \gamma)}{N^{\beta_3(R_3, \gamma)}}. \tag{2.10}$$

We fixed the parameters $\tau(R_3, \gamma)$, $B(R_3, \gamma)$, $\beta(R_3, \gamma)$ at $N = 12, 14, 16$. We checked the validity of (2.10) by comparison with our low-N data ($N = 4, 6, 8, 10$). The dashed curves in figures 1(a), 1(b) represent the resulting scaling curve $R_3(\tau, \gamma)$ for $\gamma = 0.5\pi$ and $\gamma = 0.3\pi$, respectively. The exponent $\beta_3(R_3, \gamma)$ decreases with decreasing values of R_3 and γ, which is a signal for increasing finite-size effects. This feature is easy to understand. With increasing values of τ the low-energy excitations get a stronger weight in the Laplace transform (2.2). On the other hand, the spectrum of low-energy excitations is particularly

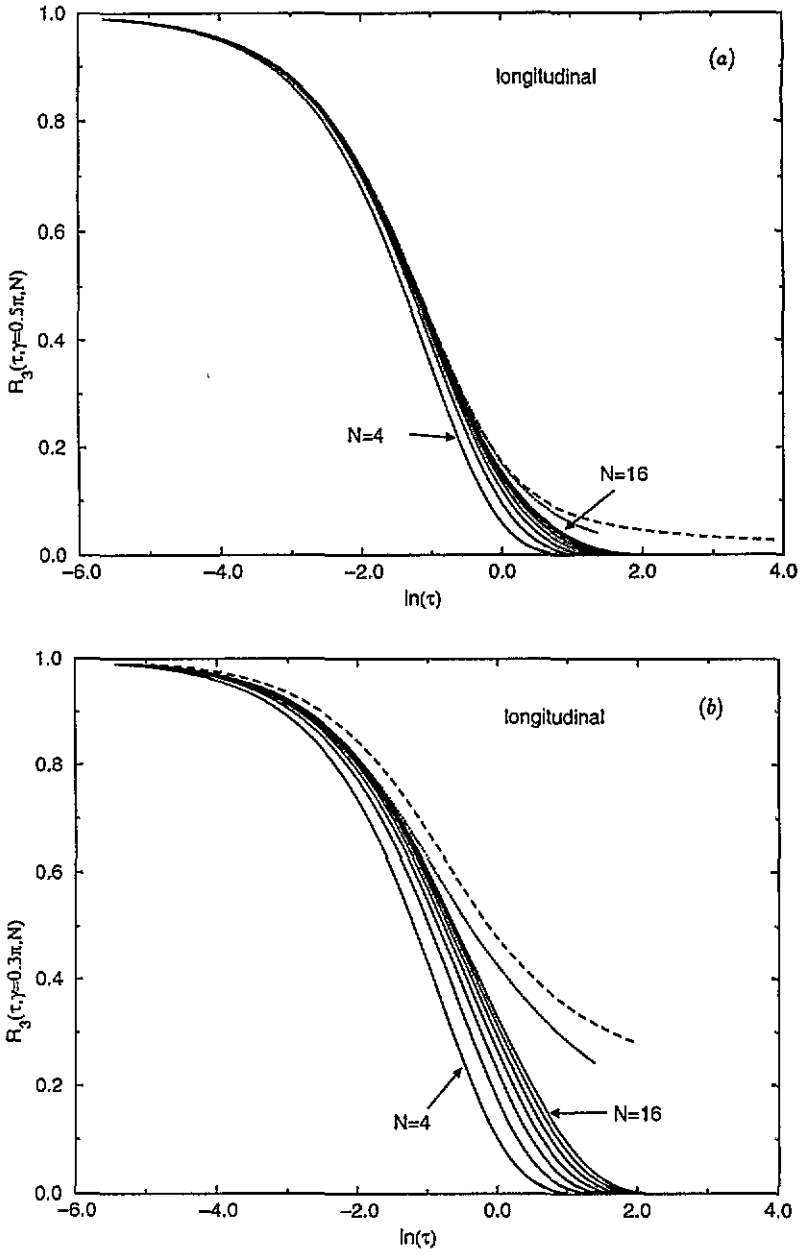

Figure 1. The ratios (2.6) of the dynamical structure factors at $p = \pi$ versus the logarithm of the euclidean time τ: (*a*) longitudinal $\gamma = \pi/2$; (*b*) longitudinal $\gamma = 0.3\pi$. The dashed curves represent the estimate of the thermodynamical limit according to (2.10). The dotted curves are the integrals (2.13).

sensitive to the finiteness of the system. We can compare our scaling curve $R_3(\tau, \gamma)$ with the *ansatz* of Müller *et al* [10] for the longitudinal structure factors:

$$S_3(\omega, p = \pi, T = 0, \gamma, N = \infty) = \frac{2A}{B(1-\alpha_3, 1/2+\alpha_3)} \frac{\Theta(\omega_2(\gamma) - \omega)}{\omega^{2\alpha_3}(\omega_2(\gamma)^2 - \omega^2)^{1/2-\alpha_3}} \qquad (2.11)$$

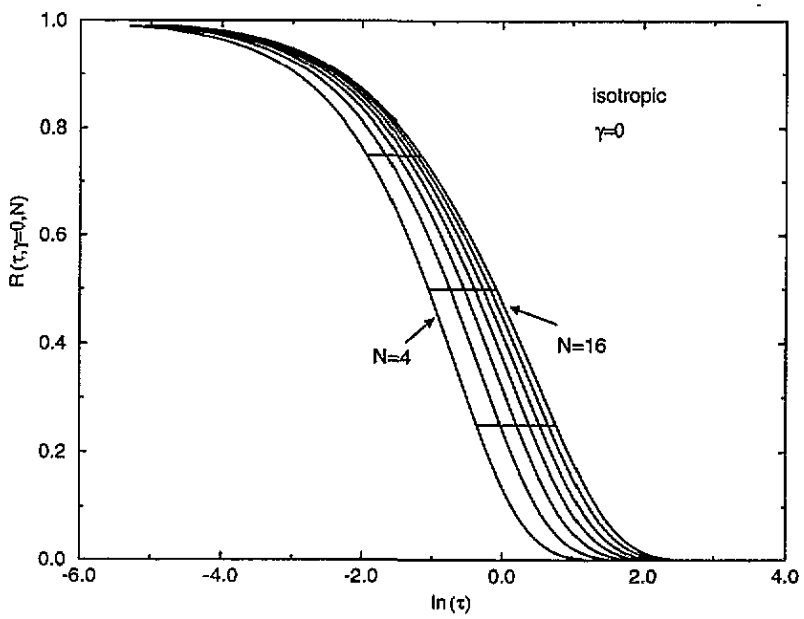

Figure 2. As figure 1, but for the isotropic case $\gamma = 0$.

where $B(x, y)$ is the beta-function. In this *ansatz* the high-frequency excitations are cut off at

$$\omega_2(\gamma) = 2\pi \frac{\sin\gamma}{\gamma}. \tag{2.12}$$

The *ansatz* coincides with the exact result of Katsura *et al* [4] in the *XX*-limit $\gamma = \pi/2$ and leads to the following expression for the ratio (2.6):

$$R_3(\tau, \gamma) = \frac{2}{B(1/2 - \alpha_3, 1/2 + \alpha_3)} \int_0^1 \mathrm{d}x\; x^{-2\alpha_3}(1 - x^2)^{\alpha_3 - 1/2} \mathrm{e}^{-x\omega_2\tau}. \tag{2.13}$$

The integral (2.13) is represented in figures 1(a),(b) by the dotted curves. For the XX-case $\gamma = \pi/2$, we find good agreement of our determination of $R_3(\tau, \gamma)$ with the exact result (2.13). This agreement supports our hypothesis, that the finite-size effects can be parametrized adequately by the *ansatz* (2.10). For $\gamma = 0.3\pi$, our finite-size analysis leads to a scaling curve $R_3(\tau, \gamma)$ which differs significantly from the prediction (2.13). This discrepancy might originate from the sharp cut-off (2.12) in the high-frequency excitations.

3. The nonintegrable infrared singularity in the transverse structure factors at $p = \pi$ and $T = 0$

Let us assume that the transverse structure factor can be split into two parts. The first one contains the nonintegrable infrared singularity ((1.4) for $j = 1$):

$$S_1(\omega, p = \pi, T = 0, \gamma, N \to \infty) = \frac{\Theta(\omega - \omega_1)}{(\omega^2 - \omega_1^2)^{\alpha_1}} \mathrm{e}^{-\omega\tau_0} \tilde{A}(\omega/\omega_1, \gamma) + S_1'(\omega, \gamma). \tag{3.1}$$

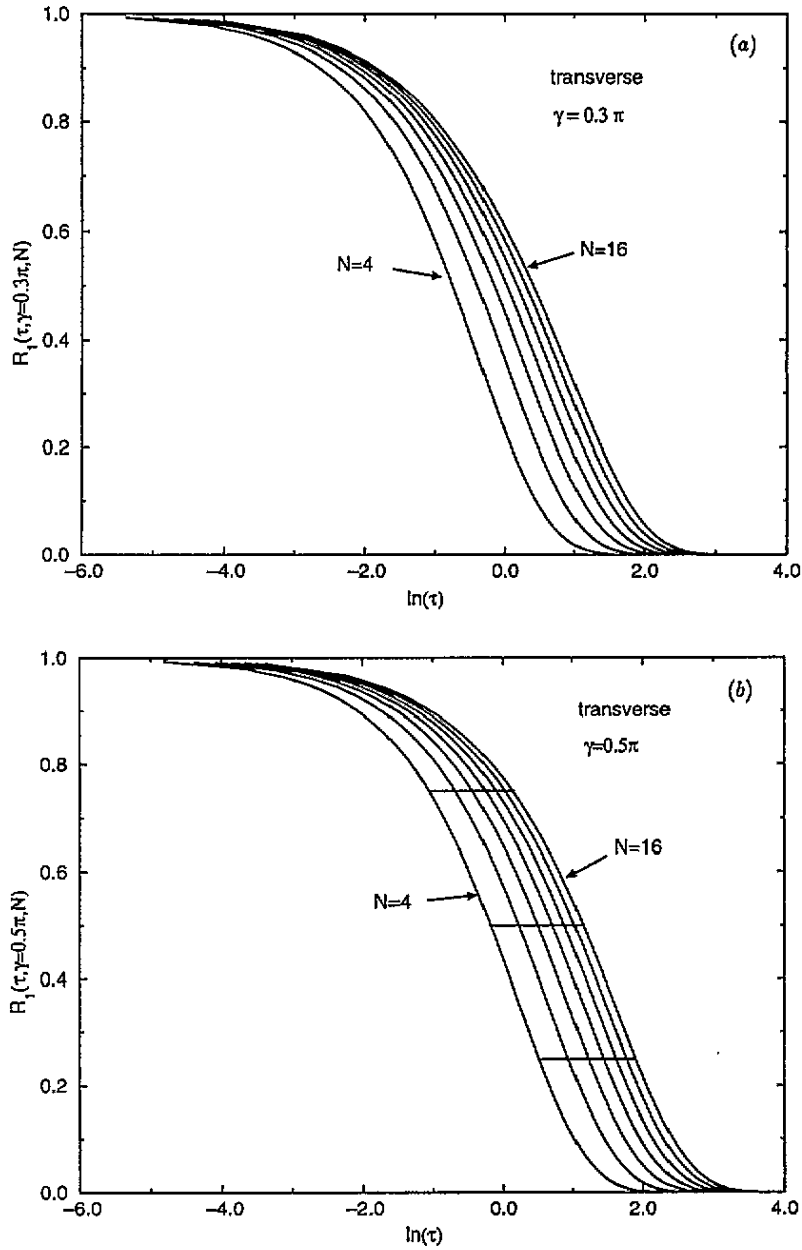

Figure 3. As figure 1, but for (*a*) transverse $\gamma = 1/3\pi$ and (*b*) transverse $\gamma = 1/2\pi$.

The second one is assumed to be free of such a singularity. We have introduced an exponential cut-off for the high-frequency contributions in the first term with a parameter τ_0, which will be fixed below. The factor $\tilde{A}(\omega/\omega_1, \gamma)$ is supposed to describe the approach to the infrared singularity. For $\omega_1 \to 0$, $\tilde{A}(\omega/\omega_1, \gamma)$ is assumed to converge to a nonvanishing value for the residue $\tilde{A}(\infty, \gamma)$ of the infrared singularity. Starting from (3.1) we find for

the ratio (2.6) in the limit $\omega_1 \to 0$:

$$R_1(\tau, \gamma, N \to \infty) = \frac{I_1(\omega_1(\tau + \tau_0), \gamma) + \omega_1^{2\alpha_1 - 1} I_1'(\tau, \gamma)}{I_1(\omega_1 \tau_0, \gamma) + \omega_1^{2\alpha_1 - 1} I_1'(0, \gamma)} \tag{3.2}$$

where

$$I_1(x, \gamma) = \int_1^\infty \mathrm{d}y\, (y^2 - 1)^{-\alpha_1} \mathrm{e}^{-xy} \tilde{A}(y, \gamma) \tag{3.3}$$

and

$$I_1'(\tau, \gamma) = \int_0^\infty \mathrm{d}\omega\, S_1'(\omega, \gamma) \mathrm{e}^{-\omega\tau}. \tag{3.4}$$

In the combined limit:

$$N \to \infty \qquad \tau \to \infty \qquad x = \omega_1(\tau + \tau_0) \quad \text{fixed} \tag{3.5}$$

we expect the ratio (3.2) to converge to a scaling function $I_1(x, \gamma)/I_1(0, \gamma)$, since $2\alpha_1 - 1 > 0$ for $0 < \gamma \leqslant \pi/2$. The scaling function (3.3) depends on the parametrization of the first contribution in (3.1). The cut-off parameter τ_0 enters in the finite-size corrections to the scaling variable x. The scaling curve depends explicitly on $\tilde{A}(y, \gamma)$. The scaling behaviour of the ratio (3.2) in the combined limit (3.5) has an immediate consequence for the 'half width':

$$\ln(\tau(R_1, \gamma, N) + \tau_0) = -\ln \omega_1(N) + \ln x(R_1, \gamma) + \ldots \tag{3.6}$$

which diverges for $N \to \infty$. Therefore on finite systems, the signature for the emergence of the nonintegrable infrared singularity is a linear increase of the half width with $\ln N$ and with slope 1. This behaviour should be observable not only for $R_1 = 0.5$ but for any fixed value of R_1 between 0 and 1. In figure 4 we have plotted the left-hand side of (3.6) with $\tau_0 = 0$ versus $-\ln \omega_1(N)$ for $R_1 = 0.75, 0.5, 0.25$ and $\gamma/\pi = 0.5$. The linear behaviour in $-\ln \omega_1(N)$ is clearly seen and the slopes 0.82, 0.92, 0.96 are found to be rather close to the expectation, namely 1. The second term in (3.6) ($x(R_1, \gamma)$) is the inverse of the scaling function $I_1(x, \gamma)/I_1(0, \gamma)$. The behaviour of the scaling function for small values of the scaling variable $x = \omega_1(\tau + \tau_0)$:

$$I_1(x \to 0, \gamma) - I_1(0, \gamma) = -\tilde{A}(\infty, \gamma)\Gamma(1 - 2\alpha_1) x^{2\alpha_1 - 1} \tag{3.7}$$

is governed by the exponent α_1 of the infrared singularity.

So far our discussion of the nonintegrable infrared singularity is restricted to the transverse case with anisotropy $\pi/2 \geqslant \gamma > 0$. In the isotropic case $\gamma = 0, \alpha_1 = \alpha_3 = 0.5$ the integral (3.3) diverges logarithmically for $x \to 0$:

$$I_1(x, \gamma = 0) = -\tilde{A}(\infty, \gamma = 0) \ln x. \tag{3.8}$$

From (3.8) we predict that the 'half width' in the isotropic case:

$$\ln[\tau(R_1, \gamma = 0, N) + \tau_0] = (R_1 - 1) \ln \omega_1(N) + C(R_1) + \ldots \tag{3.9}$$

increases with $\ln N$ but with a slope $(1 - R_1)$ depending on R_1. Again this behaviour is visible even on small systems, if we make a proper choice for $\tau_0 = 0.2$, as can be seen from figure 5. The observed slopes have the correct R_1-dependence. Their absolute value differs from the expectation by about 10%.

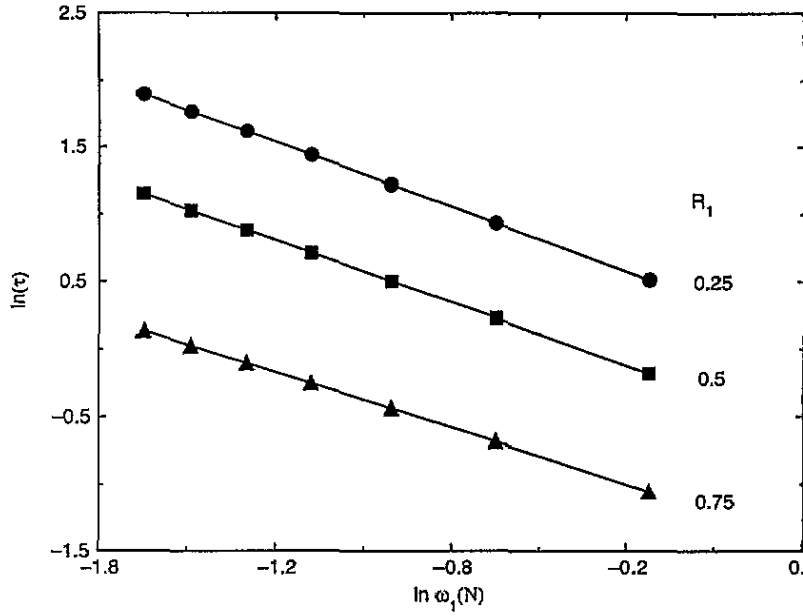

Figure 4. The finite-size behaviour of $\ln \tau$ along the horizontal lines $R_1 = 1/4, 1/2, 3/4$ shown in figure 3(*b*).

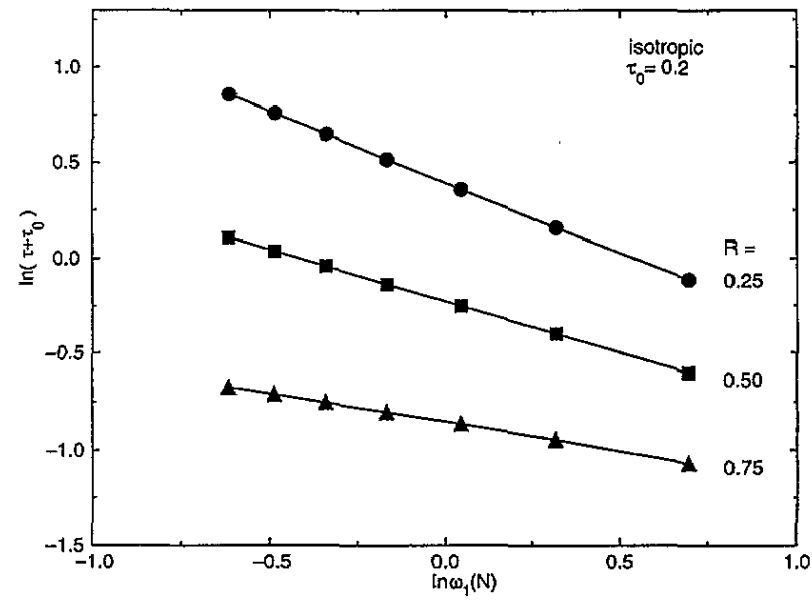

Figure 5. The finite-size behaviour of $\ln(\tau + \tau_0)$, $\tau_0 = 0.2$ along the horizontal lines $R = 1/4, 1/2, 3/4$ shown in figure 2.

4. Dynamical structure factors in the noncritical regime

Leaving the critical momentum $p = \pi$ the threshold singularities in the dynamical structure factors change in position and strength. The singularity moves according to (1.3) to

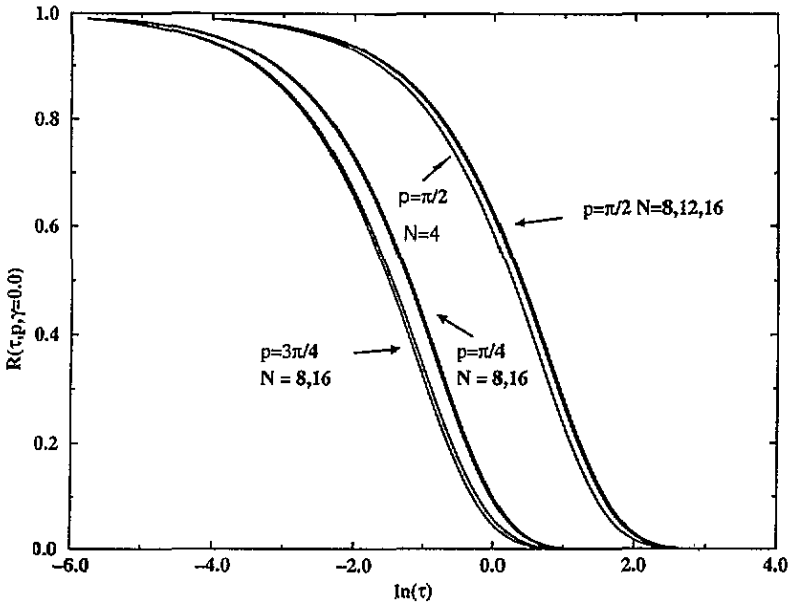

Figure 6. The ratios (4.1) of the dynamical structure factors at noncritical momenta versus $\ln \tau$: (*a*) isotropic $p/\pi = 1/4, 3/4$, $N = 8, 16$; (*b*) isotropic $p/\pi = 1/2$, $N = 4, 8, 12, 16$.

nonvanishing frequencies $\omega = \omega_1(p, \gamma)$; its strength is reduced to $(\omega - \omega_1)^{-\alpha_j}$. The threshold singularity is integrable now, since $\alpha_j < 1$ for $j = 1, 3$ and the Laplace transforms of the transverse and longitudinal structure factors exist for all nonnegative τ-values, if $0 < p < \pi$. The ratios

$$R_j(\tau, p, \gamma, N) = \frac{S_j(\tau, p, T = 0, \gamma, N)}{S_j(\tau = 0, p, T = 0, \gamma, N)} \xrightarrow{N\to\infty} R_j(\tau, p, \gamma) \tag{4.1}$$

converge to a limiting function in τ. Its large-τ behaviour is given by the threshold frequency (1.3) and the strength of the threshold singularity:

$$R_j(\tau, p, \gamma) \xrightarrow{\tau\to\infty} \exp(-\omega_1 \tau)\tau^{\alpha_j - 1}. \tag{4.2}$$

We have determined the ratios R_1 and R_3 as function of τ at fixed noncritical momenta and for various values of γ. We found extremely small finite-size effects. Moreover the ratios (4.1) almost coincide for the different values of γ and for the longitudinal and transverse case. We only observe a weak dependence on the momentum p. As an example we present in figure 6 the results for the isotropic case ($\gamma = 0$) at fixed momenta $p/\pi = 1/4, 3/4, 1/2$. The first two momenta can be realized for $N = 8, 16$. Here finite-size effects cannot be resolved in the plot of the ratio (4.1). The origin of the $\ln \tau$-axis has been shifted by 2 in order to present the results for $p = \pi/2$, $N = 4, 8, 12, 16$. Again the ratios (4.1) coincide for $N = 8, 12, 16$, whereas the result for $N = 4$ is found to the left of them.

Significant finite-size effects only appear for large values of τ and are visible in the quantities $\rho_j(t_j, \gamma, N)$ which are related to the ratios (4.1) via

$$R_j(\tau, \gamma, N) = [1 + \rho_j(t_j, \gamma, N)]^{-1} \tag{4.3}$$

where

$$t_j = \tau^{1-\alpha_j} \exp(\omega_1 \tau). \tag{4.4}$$

According to (4.2), $\rho_j(t_j, \gamma, N = \infty)$ should be linear in t_j for $t_j \to \infty$. In figure 7 we show this quantity for the isotropic case at $p = \pi/2$ and $N = 4, 8, 12, 16$. The linear behaviour in t becomes more and more apparent with increasing system size. We can compare our results for the longitudinal case with the prediction:

$$R_3(\tau, p, T = 0, \gamma) = \frac{I_3(\tau, p, \gamma)}{I_3(\tau = 0, p, \gamma)} \tag{4.5}$$

$$I_3(\tau, p, \gamma) = \int_{\omega_1}^{\omega_2} d\omega \ (\omega^2 - \omega_1^2)^{-\alpha_3}(\omega_2^2 - \omega^2)^{-1/2+\alpha_3} e^{-\omega\tau} \tag{4.6}$$

which follows from the *ansatz* of Müller *et al* [10]. In (4.6) the lower and upper integration bounds are given by (1.3) and

$$\omega_2(p, \gamma) = \frac{2\pi}{\gamma} \sin\gamma \sin\frac{p}{2}, \tag{4.7}$$

respectively. The prediction is found between the finite-system results for $N = 12$ and $N = 16$ (cf. the dotted curve in figure 7). Better agreement with the expected behaviour in the thermodynamical limit can be achieved for example by lowering the upper integration bound ω_2 in equation (4.6). This, however, would violate the sum rules of [13]. To our knowledge there does not yet exist a generalization of the *ansatz* of Müller *et al* [10], which respects the sum rules in [13].

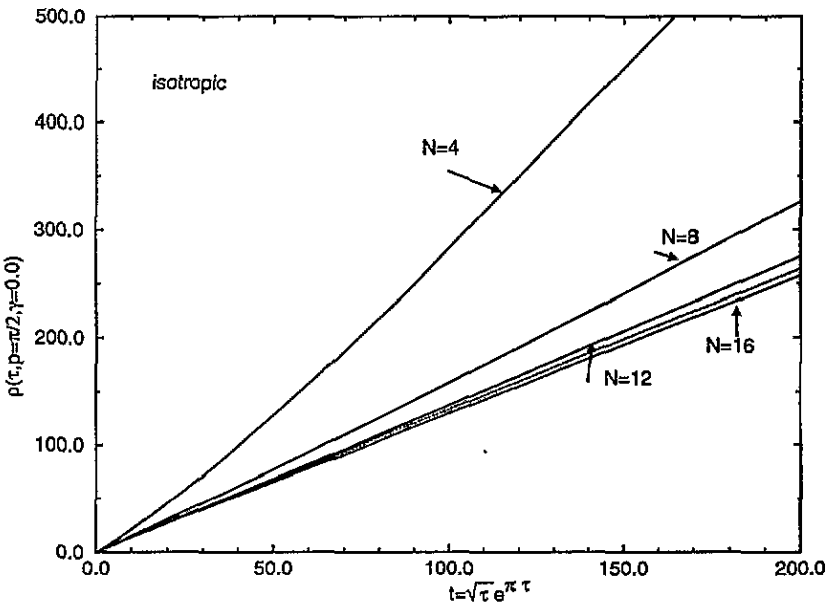

Figure 7. The quantity $\rho(t, p = \pi/2, \gamma = 0, N)$—defined in (4.3)—versus t—defined in (4.4). The dashed curve is the prediction (4.5), (4.6).

In figure 8 we show the ratio R as function of the momentum p $(0 < p < \pi)$ and at fixed $\tau = 0.5$, $\gamma/\pi = 0.0$, $N = 4, 6, \ldots 16$. All these data points nicely follow one curve in the 'scaling' variable p. Again this means that the thermodynamical limit is seen already on small systems.

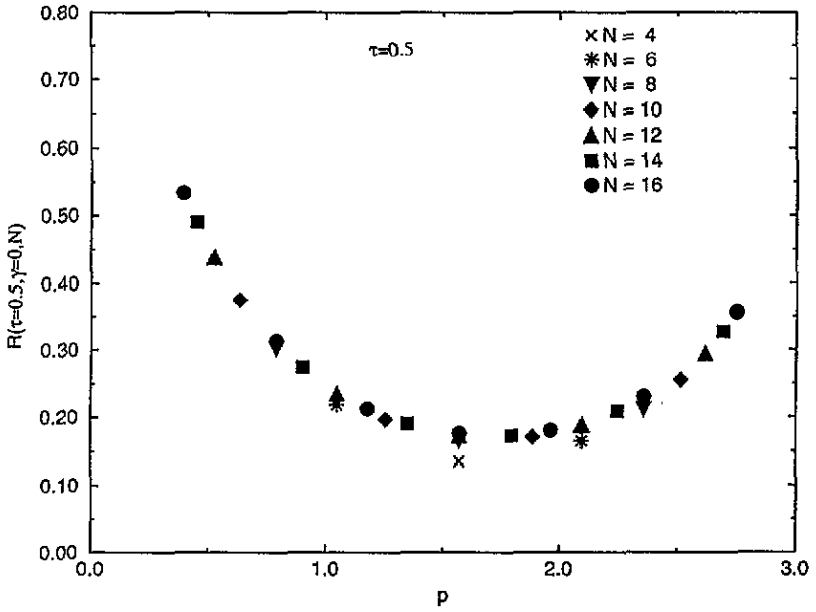

Figure 8. The ratio (4.1) of the dynamical structure factors at fixed euclidean time $\tau = 0.5$ versus momentum p and for $N = 4, 6, \ldots, 16$.

5. Conclusions

In this paper we started a first attempt to extract the dynamical structure factors of the *XXZ*-model from a complete diagonalization of the Hamiltonian on finite rings with $N = 4, 6, \ldots 16$ sites. We studied the normalized ratios (2.6) of the dynamical structure factors as function of the euclidean (imaginary) time τ and found the following features:

(i) Away from the critical momentum $p = \pi$ finite-size effects are small except for in the large-τ limit, where we find a clean signal for the threshold singularity (1.4).

(ii) At the critical momentum $p = \pi$ finite-size effects are still small in the longitudinal case at $\gamma = \pi/2$ but increase for decreasing values of γ. These finite-size effects can be described adequately by the *ansatz* (2.10). The resulting thermodynamical limit (2.9) for the ratio (2.6) is in good agreement with the exact result of Katsura *et al* [4] at $\gamma = \pi/2$ but deviates from the prediction (2.13) of Müller *et al* [10] for smaller values of γ.

(iii) At the critical momentum $p = \pi$ finite-size effects are large in the transverse case and increase rapidly with increasing values of γ. It was demonstrated in section 3 that this behaviour signals the emergence of the (nonintegrable) infrared singularity in the transverse structure factor.

Therefore we can conclude that the euclidean time representation is particularly suited for the study of finite-size effects, which allows for a crude estimate of the thermodynamical limit. This estimate is already precise enough to check the gross features of a model *ansatz* [10] for the dynamical correlation functions in the spectral (ω-) representation. To resolve the fine structure, however—i.e. the detailed form and cut-off of the nonsingular contributions—one has to know the euclidean time dependence very precisely. In other words: The reconstruction of the spectral (ω-) representation from the euclidean time (τ-) representation demands for an analytic continuation and tiny errors in the τ-representation

might produce large errors in the ω-representation. Of course this problem would not occur if finite-size effects could be analysed systematically in the spectral representation. The continued-fraction method used in [14] might open up this possibility.

Our exact results on small systems might be useful as a test for those, who plan to develop approximative calculations on larger systems. For this purpose we present in appendix A our results for the first nine excitation energies with the corresponding transition probabilities at fixed $p/\pi = 1/4, 1/2, 3/4, 1$; $N = 16$; $\gamma = 0$.

Appendix A. Excitation energies and transition probabilities for $N = 16$

In table A1 we present the excitation energies $\omega_n = E_n - E_0$ and the transition probabilities $t_n = |\langle n|s_3(0)|0\rangle|^2$ for the isotropic case at fixed momenta $p/\pi = 1/4, 1/2, 3/4, 1$.

Table A1.

$S(\tau = 0, p = \pi/4) = 2.982\,766\,323\,178\,24 \times 10^{-1}$		$S(\tau = 0, p = \pi/2) = 0.679\,437\,576\,126\,672$	
$\omega_n(\pi/4)$	$t_n(\pi/4)$	$\omega_n(\pi/2)$	$t_n(\pi/2)$
2.302 618 995 384 36	$2.942\,376\,044\,483\,45 \times 10^{-1}$	3.380 661 385 889 31	$5.845\,576\,165\,882\,52 \times 10^{-1}$
4.293 058 678 578 73	$3.263\,179\,365\,395\,63 \times 10^{-4}$	4.197 135 363 571 46	$8.753\,351\,302\,481\,42 \times 10^{-2}$
4.550 193 770 432 69	$2.558\,961\,696\,679\,15 \times 10^{-3}$	4.597 570 742 552 91	$4.164\,845\,049\,348\,24 \times 10^{-3}$
5.003 738 640 110 45	$2.168\,974\,225\,540\,17 \times 10^{-4}$	4.738 715 285 730 11	$1.009\,619\,502\,275\,32 \times 10^{-3}$
5.568 925 689 320 23	$8.328\,765\,422\,592\,78 \times 10^{-5}$	4.902 809 151 018 72	$6.608\,972\,186\,818\,34 \times 10^{-5}$
5.781 393 387 220 18	$1.307\,021\,933\,214\,60 \times 10^{-4}$	5.351 326 977 942 61	$1.170\,910\,176\,488\,93 \times 10^{-4}$
5.845 005 694 549 30	$4.978\,800\,138\,583\,12 \times 10^{-4}$	5.890 305 368 733 91	$2.048\,316\,977\,965\,75 \times 10^{-4}$
6.290 136 187 145 56	$2.134\,547\,712\,462\,74 \times 10^{-5}$	5.929 019 858 388 70	$1.274\,343\,354\,700\,92 \times 10^{-3}$
6.332 121 438 692 86	$1.260\,960\,122\,860\,78 \times 10^{-5}$	6.475 753 895 114 23	$5.635\,173\,506\,832\,56 \times 10^{-5}$
$S(\tau = 0, p = 3\pi/4) = 1.32305343430234$		$S(\tau = 0, p = \pi) = 4.29230350827985$	
$\omega_n(3\pi/4)$	$t_n(3\pi/4)$	$\omega_n(\pi)$	$t_n(\pi)$
2.638 130 434 568 11	1.021 021 983 181 91	0.540 379 364 500 57	3.439 616 887 898 93
3.411 532 042 825 32	$1.025\,452\,373\,356\,83 \times 10^{-3}$	2.792 061 172 198 89	$6.056\,078\,903\,245\,50 \times 10^{-1}$
4.330 655 742 114 27	$2.457\,520\,878\,288\,75 \times 10^{-1}$	4.668 596 605 332 13	$2.004\,161\,016\,515\,47 \times 10^{-1}$
5.035 832 362 017 23	$1.188\,797\,549\,291\,33 \times 10^{-3}$	5.475 947 091 450 50	$7.023\,054\,488\,151\,08 \times 10^{-4}$
5.440 678 860 837 06	$5.871\,093\,211\,458\,63 \times 10^{-4}$	5.907 016 581 348 04	$4.485\,036\,273\,125\,39 \times 10^{-2}$
5.462 702 978 578 87	$5.226\,289\,900\,552\,92 \times 10^{-2}$	5.994 081 786 221 40	$4.454\,485\,992\,790\,42 \times 10^{-6}$
5.980 403 221 359 34	$1.068\,842\,349\,828\,29 \times 10^{-4}$	6.573 253 456 022 60	$6.661\,055\,818\,870\,54 \times 10^{-4}$
6 445 855 721 184 17	$3.080\,526\,033\,945\,93 \times 10^{-5}$	6.802 832 461 833 18	$2.876\,991\,287\,862\,44 \times 10^{-4}$
6.643 038 641 264 50	$7.254\,113\,180\,587\,85 \times 10^{-4}$	7.144 627 849 407 82	$1.980\,761\,774\,949\,86 \times 10^{-6}$

References

[1] Fabricius K, Löw U, Mütter K-H and Ueberholz P 1991 *Phys. Rev.* B **44** 7476
Fabricius K, Löw U and Mütter K-H 1993 *Z. Phys.* B **91** 51

[2] Fabricius K, Löw U and Mütter K-H 1995 Complete solution of the *XXZ*-model on finite rings. Finite temperature structure factors *Phys. Rev.* B **51** 8270

[3] Niemeijer T 1967 *Physica* **36** 377

[4] Katsura S, Horiguchi T and Suzuki M 1967 *Physica* **46** 67

[5] Mazur P and Siskens T J 1973 **69** 259 ; 1974 *Physica* **71** 560

[6] Barouch E, McCoy B M and Abraham D B 1971 *Phys. Rev.* A **4** 2331
McCoy B M, Perk J H H and Schrock R E 1983 *Nucl. Phys.* B **220 [FS8]** 35
Müller G and Schrock R E 1984 *Phys. Rev.* B **29** 228

Stolze J, Nöppert A and Müller G 1995 Gaussian, exponential and power-law decay of time-dependent correlation functions in quantum spin chains *Phys. Rev.* B submitted

[7] Lieb E, Schultz T and Mattis D 1961 *Ann. Phys., NY* **16** 407

[8] des Cloizeaux J and Pearson J J 1962 *Phys. Rev.* **128** 2131

[9] Luther A and Peschel I 1975 *Phys. Rev.* B **12** 3908
Fogedby H C 1978 *J. Phys. C: Solid State Phys.* **11** 4767

[10] Müller G, Thomas H, Puga M W and Beck H 1981 *J. Phys. C: Solid State Phys.* **14** 3399
Müller G, Thomas H, Beck H and Bonner J C 1981 *Phys. Rev.* B **24** 1429

[11] Tennant D A, Perring T G, Cowley R A and Nagler S E 1993 *Phys. Rev. Lett.* **70** 4003

[12] Karbach M, Mütter K-H and Schmidt M 1994 *Phys. Rev.* B **50** 9281

[13] Müller G 1982 *Phys. Rev.* B **26** 1311

[14] Viswanath V S, Zhang S and Müller G 1994 *Phys. Rev.* B **49** 9702
Viswanath V S and Müller G 1994 *The Recursion Method—Application to Many-Body Dynamics (Springer Lecture Notes in Physics 23)* (Berlin: Springer)